2006 IEEE International
Symposium on Signal Processing
and Information Technology

Bilateral Filtering of Diffusion Tensor MR Images

Ghassan Hamarneh and Judith Hradsky
Medical Image Analysis Lab, School of Computing Science, Simon Fraser University
Burnaby, BC, V5A 1S6, Canada

Abstract— **In this paper we present a bilateral image filtering algorithm for edge-preserving smoothing of diffusion tensor magnetic resonance imaging (DTMRI) data. The bilateral filtering is performed in the Log-Euclidean framework which guarantees valid output tensors. Smoothing is achieved by weighted averaging of neighboring tensors. Analogous to bilateral filtering of scalar images, the weights are chosen to be inversely proportional to two distance measures: The geometrical Euclidean distance between the spatial locations of tensors and the dissimilarity of tensors. The following methods for tensor dissimilarity measures are compared: The Log-Euclidean, the similarity-invariant Log-Euclidean, the square root of the J-divergence, and the distance scaled mutual diffusion coefficient. We describe the non-iterative DT smoothing equation in closed form. Interpolation of DT data is treated as a special case of bilateral filtering where only spatial distance is used. We present qualitative and quantitative smoothing and interpolation results on both synthetic tensor field data and real cardiac and brain DTMRI data.**

I. Introduction

Diffusion is the process by which molecules are transported from one part of a medium to another. The flux of diffusing molecules is a result of their random Brownian motion in concentration gradients and is described by Fick's law. Diffusion tensor magnetic resonance imaging (DTMRI) records the diffusion characteristics of water molecules along fiber tracts in-vivo and is becoming increasingly valuable for assessing the effects of disease progression and treatment evaluation on fiber connectivity and diffusion properties [1], [2]. In DTMRI, typically each voxel of the 3D image is assigned a rank three, second order diffusion tensor forming a 3D tensor field. Each tensor is expressed as a 3×3 symmetric, positive semi-definite (PSD) matrix (with nonnegative eigenvalues). The general classes of medical image processing and analysis algorithms performed on scalar medical images (e.g. filtering, segmentation, registration and visualization of X-ray CT, T1-weighted MRI, ultrasound, and others) need to be extended to DTMRI tensor fields in order to glean quantitative and qualitative information, potentially improving computer aided diagnosis, follow up of treatment and disease progression, and statistical analysis of structural and functional variability. In the following paragraphs we review important contributions in processing, segmentation, and registration of tensor field data.

The primary goal of processing is to reduce the noise in the DTMRI data that occurs due to various imaging acquisition artifacts. There exist numerous techniques for image processing of scalar fields; an essential task in any image processing pipelines. However, only a few methods have been recently extended to perform basic processing and reduce noise in diffusion tensor image data; for example median filtering, morphological operations, interpolation, and anisotropic edge preserving smoothing [3], [4], [5], [6].

Identifying and delineating regions of interest (ROI) in image data is necessary for performing subsequent quantitative analysis and qualitative visualization. Segmentation methods typically rely on (a) identifying nearby voxels with similar diffusion properties and grouping them into one coherent structure, (b) identifying edges in the images and linking them to form separating boundaries between neighboring structures, and (c) incorporating prior knowledge about the shape characteristics of the different target structures to segment. These intuitive ideas are very well understood for the scalar case, but have only recently been the focus of research for tensor fields [7], [8], [9], [10], [11], [12], [13], [14], [15], [16].

To facilitate viewing and interrogating DTMRI segmentation and visualization results within the context of other medical imaging modalities (e.g. structural MRI), the data sets must be properly fused by bringing them into proper spatial alignment. Image registration is also needed for quantitative and qualitative longitudinal analysis tasks in which DTMRI data of the same subject at different times must be compared [17], [18], [19], [20].

In this paper we propose a bilateral diffusion tensor filtering algorithm, which carries the same intuitive ideas as of its scalar field counterpart. Towards this goal, tensors must be averaged appropriately without producing invalid tensors, and similarity between tensor values must be calculated in a meaningful way. In order to realize this extension, we make use of two major recent advancements in the field of DTMRI processing, namely tensor calculus and diffusion tensor dissimilarity measures.

The remainder of the paper is organized as follows. Following a brief review of bilateral filtering for scalar images in section II, we propose the closed form solution for bilateral filtering of DT fields and describe its reliance on the Log-Euclidean framework and the tensor dissimilarity measures. In section III, we present smoothing and interpolation results on synthetic and real data. We summarize and draw conclusions in section IV.

II. Bilateral Filtering of DTMRI

A. Bilateral Filtering of Scalar Images

Bilateral filtering smoothes image data while preserving edges by means of a nonlinear combination of nearby image values [21]. For an input image $f(x)$, the filtered output image

$h(x)$ is defined as follows:

$$h(x) = k^{-1}(x) \int_{-\infty}^{\infty} \int_{-\infty}^{\infty} f(\xi) c(\xi, x) s(f(\xi), f(x)) d\xi \quad (1)$$
$$k(x) = \int_{-\infty}^{\infty} \int_{-\infty}^{\infty} c(\xi, x) s(f(\xi), f(x)) d\xi$$

where $c(\xi, x)$ is inversely proportional to the spatial distance between the neighbourhood center x and a nearby location ξ, and $s(f(\xi), f(x))$ is the photometric similarity (e.g. in grey level values) between the image function at x and ξ. This essentially means that image values with closer spatial and photometric proximity contribute more to the output filtered pixel by having a higher weight in a weighted-average implementation. Trilateral filtering has been recently proposed to take texture of scalar intensity images into account as well [22].

For DTMRI data, calculating the spatial proximity (Euclidean distance) of tensors in the image domain clearly remains the same as in the scalar case. However, two important operations must be redefined for tensor fields, namely, weighted-averaging of DTs and calculating tensor dissimilarity.

B. Weighted Averaging of Diffusion Tensor

Diffusion tensors do not form a vector space since they are symmetric PSD matrices whose space is restricted to a convex half-cone [23]. Therefore, special care needs to be taken when performing calculations and statistics on diffusion tensors. For example, simply subtracting two DTs in general gives an invalid DT [24], [23]. Arsigny *et al* recently proposed the Log-Euclidean Riemannian framework allowing simple tensor computations in the domain of matrix logarithms [25]. Specifically, for the proposed extension of bilateral smoothing to tensor fields, the weighted average of tensors is given by:

$$T(x) = k(x)^{-1} exp\left(\sum_{i=1}^{N} w_i(x) log(T(\xi_i))\right) \quad (2)$$

$$k(x) = \sum_{i=1}^{N} w_i(x) \quad (3)$$

where $T(x)$ is the tensor resulting from averaging N tensors, $T(\xi_i)$, in the neighbourhood of x with corresponding weights w_i. exp and log denote matrix exponential and logarithm, respectively. To perform DT smoothing, equation (2) is applied at each location x in the image and each tensor $T(x)$ is replaced by a weighted average of N neighboring tensors $T(\xi_i)$. For example, N=9 for a 3×3 8-connected 2D neighbourhood, and N=27, for a $3 \times 3 \times 3$ 26-connected 3D neighbourhood.

C. Bilateral Filtering of Diffusion Tensors

The smoothing effect now clearly depends on the choice of the weights, w_i. A simple implementation of (equal-weight) averaging is achieved by setting $w_i = 1/N$ for all i. However, this operation blurs interfaces between tissues of different diffusion properties; e.g. white and gray matter in the brain. This is where the bilateral filtering ideas are essential for edge-preserving smoothing. Towards this end, to replace the tensor at each pixel in the image, we define the weights to be inversely proportional to the spatial distance and to the tensor dissimilarity between the neighboring tensors and the center tensor, according to

$$w_i(x) = \alpha f_1(d_T(T(x), T(\xi_i))) + (1 - \alpha) f_2(d_S(x, \xi_i)) \quad (4)$$

where $d_T(T(x), T(\xi_i))$ is the tensor dissimilarity between $T(x)$ and $T(\xi_i)$, $d_S(x, \xi_i)$ is the spatial euclidean distance between x and ξ, f_1 and f_2 are monotonically decreasing functions that map the range of tensor-dissimilarity values and spatial distances, respectively, to the interval $[0, 1]$, and $\alpha \in [0, 1]$ controls the relative emphasis on spatial versus tensor distance.

D. Diffusion Tensor Dissimilarity

What remains is a proper definition of tensor dissimilarity, $d_T(T_1, T_2)$, between two tensors, T_1 and T_2. The Frobenius norm, $\|T_1 - T_2\|_F$, where $\|A\|_F = \sqrt{Tr(AA^H)}$, would be an obvious choice had the diffusion tensors spanned a Euclidean space. However, given the PSD nature of the diffusion tensors, such measure of dissimilarity is inappropriate.

We adopt and compare (see section III) four approaches proposed recently for calculating tensor dissimilarity in the proposed bilateral diffusion filtering algorithm: The Log-Euclidean distance, the similarity-invariant Log-Euclidean distance [25], the affine-invariant square root of the J-divergence [8], and the distance scaled mutual diffusion coefficient [26], denoted respectively as $d_{T_{LE}}$ and $d_{T_{LEI}}$, d_{T_J}, and d_{T_K} and are given by

$$d_{T_{LE}}(T_1, T_2) = \|log(T_1) - log(T_2)\| \quad (5)$$

$$d_{T_{LEI}}(T_1, T_2) = \sqrt{Tr((log(T_1) - log(T_2))^2)} \quad (6)$$

$$d_{T_J}(T_1, T_2) = \frac{1}{2}\sqrt{Tr(T_1^{-1}T_2 + T_2^{-1}T_1) - 2n} \quad (7)$$

$$d_{T_K}(T_1, T_2) = \frac{[(v'T_1v)(v'T_2v)]^{\gamma}}{\sigma^2} \quad (8)$$
$$v = (x_1 - x_2)/\sigma, \sigma = \|x_1 - x_2\|, \gamma = 1,$$

where x_i describes the location of T_i (see [26] for details), and n is the size of the square tensor, i.e. $n = 3$ in 3D DTMRI images.

The resulting method is a closed-form, edge-preserving filtering extending the original scalar bilateral filter to diffusion tensor data. The method is non-iterative, nevertheless, multiple smoothing iterations can still be performed as is typical in scalar image filtering algorithms. Further, we handle diffusion tensor field interpolation as a special case of bilateral filtering (equation (2)) as follows. We interpolate a tensor at any non-grid position as the Log-Euclidean weighted sum of N nearby tensors, $T(\xi)$, where the weights are inversely proportional to the spatial distance between the non-grid position x and the locations of the nearby tensors, ξ. This is intuitively and conveniently obtained by setting $\alpha = 0$ in equation (4). We also note that it is straightforward to generalize the proposed method to any dimension.

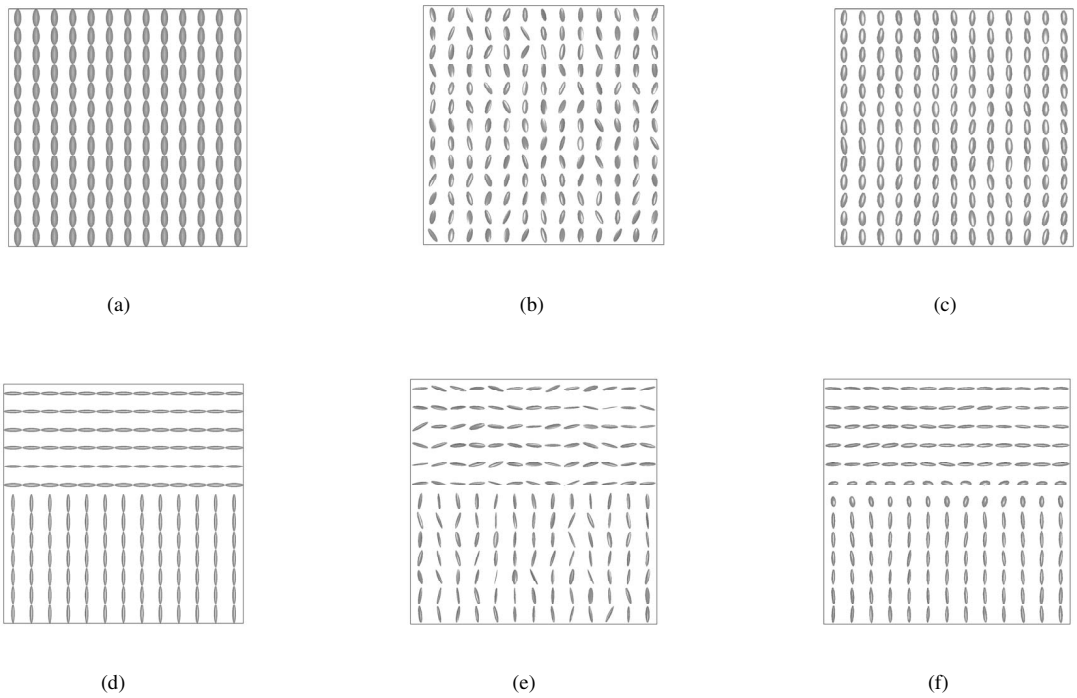

(a) (b) (c)

(d) (e) (f)

Fig. 1. Smoothing on two synthetic tensor fields. a) shows the original homogenous tensor field, d) shows another original tensor field that contains the interface. b) and e) show the noisy version of a) and d) respectively, while c) and f) show the smoothing results on b) and e). d_{T_J}, $\alpha = 1$, $N = 9$ are used as an example. The effect of changing these parameters are shown in other figures.

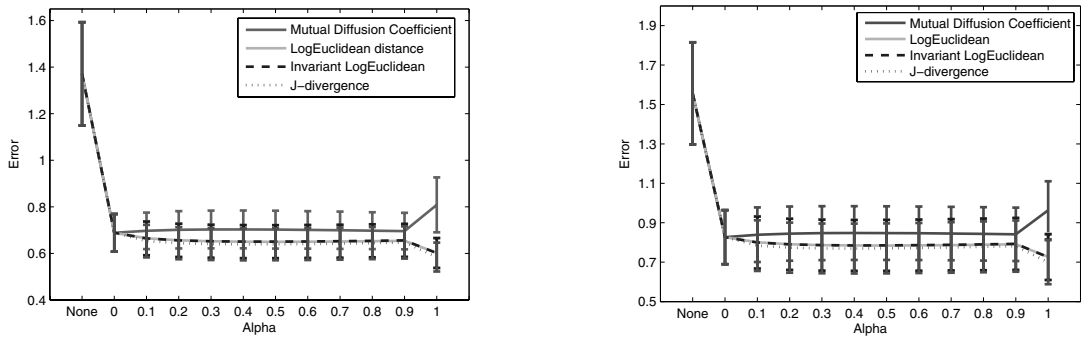

(a) (b)

Fig. 2. Effect of α on the denoising of synthetic data. Mean error values shown are calculated by averaging all the tensor distances between corresponding pixels in the denoised image and the original image. Mean and standard deviation of error are shown for different values of α. The first error entry (at "None") represents the error of the noisy image. The error results are measured using d_{T_J} for (a) the homogeneous tensor field (Figure 1b) and for (b) the DT field with the interface (Figure 1e). Fig. 4 may be useful to relate these distances to tensors differences.

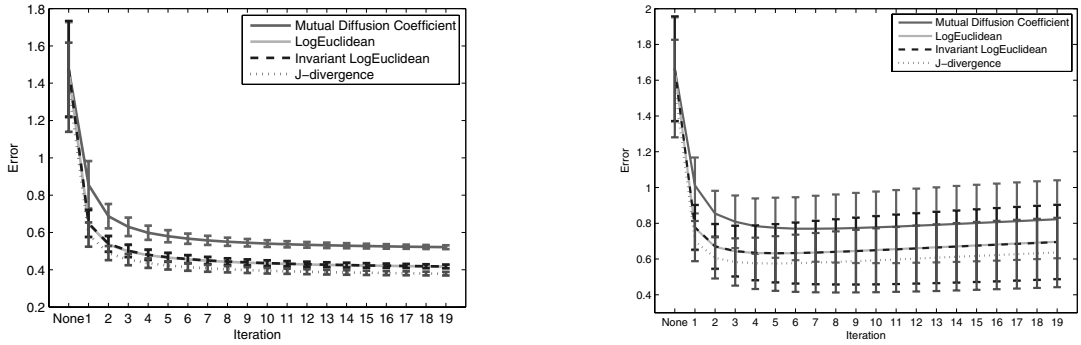

(a) (b)

Fig. 3. Effect of number of iterations on bilateral DT smoothing. This figure depicts the error values as the number of bilateral filtering iterations is increased, from 1 to 19 iterations. Iteration 0 corresponds to the noisy image without filtering. The error is calculated as the average tensor distance between the smoothed and the original image. Note the sharp decrease in error in the first 5 iterations. In (a) the original image did not contain any clear boundaries whereas (b) contained a clear edge (similar to Fig. 1e). Note how in (b) the error begins to increases slightly due to blurring the edge if an excessive number of iterations is performed.The error is measured using d_{T_J}, $\alpha = 1$, and $N = 9$.

Tensor	1	2	3	4	5	6	7	8	9	10	11	12	13	14	15	16	17	18	19	20
1	0	1.1619	2.1909	0.67082	1.2649	0.67082	1.2649	0.67082	1.2649	0.83666	1.2649	0.83666	1.2649	0.83666	1.2649	0.83666	1.2649	1.2302	1.8923	0.60885
2	0.91629	0	0.86603	0.94868	1.0724	0.94868	1.0724	0.94868	1.0724	1.4318	1.0724	1.4318	1.0724	1.4318	1.0724	1.4318	1.0724	0.33531	3.3782	1.3808
3	1.6094	0.69315	0	1.8574	1.7889	1.8574	1.7889	1.8574	1.7889	2.429	1.7889	2.429	1.7889	2.429	1.7889	2.429	1.7889	0.94354	5.0241	2.4099
4	0.91629	0.91629	1.6094	0	0.5	0.94868	1.4318	0.94868	1.4318	1.0724	1.0724	1.0724	1.0724	1.0724	1.4318	1.0724	1.0724	0.89026	2.0401	0.742
5	1.6094	0.91629	1.6094	0.69315	0	1.4318	1.7889	1.4318	1.7889	1.5811	1.2649	1.5811	1.2649	1.5166	1.7889	1.5811	1.2649	0.93088	2.3423	1.1729
6	0.91629	0.91629	1.6094	0.91629	1.6094	0	0.5	0.94868	1.4318	1.0724	1.0724	1.0724	1.0724	1.0724	1.0724	1.0724	1.4318	1.1278	2.1431	1.2899
7	1.6094	0.91629	1.6094	1.6094	1.6094	0.69315	0	1.4318	1.7889	1.5811	1.2649	1.5811	1.2649	1.5811	1.2649	1.5166	1.7889	1.3042	2.5749	2.0082
8	0.91629	0.91629	1.6094	0.91629	1.6094	0.91629	1.6094	0	0.5	1.0724	1.4318	1.0724	1.4318	1.0724	1.0724	1.0724	1.0724	1.0367	3.1335	0.65854
9	1.6094	0.91629	1.6094	1.6094	1.6094	1.6094	1.6094	0.69315	0	1.5166	1.7889	1.5166	1.7889	1.5811	1.2649	1.5811	1.2649	1.1617	4.504	1.0679
10	0.91629	1.6094	2.3026	1.2726	1.8312	1.2726	1.8312	0.91629	1.6094	0	0.70711	1.7889	2.1213	1.2247	1.5492	1.2247	1.5492	1.4825	2.0792	1.0515
11	1.6094	0.91629	1.6094	1.2726	1.138	1.2726	1.138	1.6094	1.6094	0.69315	0	2.1213	1.7889	1.5492	1.5492	1.5492	1.5492	1.1151	2.4178	1.5882
12	0.91629	1.6094	2.3026	1.2726	1.8312	1.2726	1.8312	0.91629	1.6094	1.6094	2.3026	0	0.70711	1.2247	1.5492	1.2247	1.5492	1.5146	2.1464	1.1649
13	1.6094	0.91629	1.6094	1.2726	1.138	1.2726	1.138	1.6094	1.6094	2.3026	1.6094	0.69315	0	1.5492	1.5492	1.5492	1.5492	1.1507	2.5041	1.6988
14	0.91629	1.6094	2.3026	0.91629	1.6094	1.2726	1.8312	1.2726	1.8312	1.1435	1.7376	1.1435	1.7376	0	0.70711	1.2247	1.5492	1.2921	2.9232	0.9518
15	1.6094	0.91629	1.6094	1.6094	1.6094	1.2726	1.138	1.2726	1.138	1.7376	1.3838	1.7376	1.3838	0.69315	0	1.5492	1.5492	1.0462	4.2263	1.4578
16	0.91629	1.6094	2.3026	1.2726	1.8312	0.91629	1.6094	1.2726	1.8312	1.1435	1.7376	1.1435	1.7376	1.1435	1.7376	0	0.70711	1.4736	2.4758	1.0302
17	1.6094	0.91629	1.6094	1.2726	1.138	1.6094	1.6094	1.2726	1.138	1.7376	1.3838	1.7376	1.3838	1.7376	1.3838	0.69315	0	1.0186	3.6085	1.1404
18	1.1647	0.37774	1.0709	1.0559	1.0557	1.1643	1.1642	1.1605	1.1602	1.6729	1.0997	1.6934	1.07	1.2777	1.162	1.7221	1.0804	0	3.5633	1.2765
19	2.1999	3.1162	3.8094	2.2002	2.2009	2.3168	2.5227	3.0641	3.7345	2.2347	2.3739	2.2503	2.4183	2.8926	3.5856	2.5758	3.2385	3.2186	0	2.4753
20	0.67991	1.5862	2.2893	0.72319	1.3448	1.5825	2.2715	0.76587	1.2579	1.1886	1.8769	1.2951	1.9653	1.0659	1.7578	1.0717	1.31	1.3816	2.6114	0

Fig. 4. Diffusion Tensor Distances. (top row) A variety of DTs visualized using the common 3D ellipsoidal glyph whose orientations are given by the eigenvectors and the length of their semi-axes by the eigenvalues of the DT. (second row) $d_{T_{LE}}$ and d_{T_J} (lower and upper triangle respectively) distances between pairs of ellipsoids. The first three DTs (1, 2, 3) are isotropic with $\lambda = 1, 2.5, 5$. The next three pairs (4-5, 6-7, 8-9) have $\lambda_1 = 5$ or 2.5, and $\lambda_2 = \lambda_3 = 1$, and are oriented along x, y, and z, respectively. The next four pairs (10-11, to 16-17) are 45-rotated versions of tensors 4 to 9. The last three tensors are randomly selected real DTMRI tensors.

III. Experiments and Results

The proposed DT bilateral filtering is developed as an integral preprocessing step for segmentation and analysis of DTMRI data related to two long term clinical applications. Firstly, we are investigating the effect of disease progression and treatment in multiple sclerosis patients on inter-hemispheric fiber connectivity and diffusion properties within different regions of the callosum (CC) bridge [27], [28]. Secondly, we are studying the properties of the laminar cardiac fiber sheet in the myocardium from DTMRI.

In this section we present qualitative and quantitative smoothing and interpolation results of synthetic tensor fields as well as real cardiac and brain DTMRI data.

For validating our work as shown in subsections III-A and III-B, we made use of two synthetic data sets. The first data set contains a homogeneous DT field whereas the other contains a clear interface between two regions with different diffusion properties (Fig. 1). Noisy DTMRI images were produced by adding random Gaussian noise independently to the three eigen values (as in [3]), in addition to random rotation (in azimuth and elevation) perturbing the three eigen vectors by the same amount to retain orthogonality.

Error calculations are obtained by creating 10 noisy images, smoothing them with different values of α or over several iterations, and estimating the mean error and standard derivation of the difference between the smoothed DT field to the (known) noise-free original. This is done for three different tensor measures. The error difference is calculated by averaging all the tensor distances between corresponding pixels in the denoised image and the original image.

A. Effect of Alpha on Bilateral DT-Smoothing

The noisy images are smoothed using α ranging from 0.0 to 1.0 in increments of 0.1 (Fig. 2). This was done for all distance measures and both mapping functions. Similar results are obtained when using different tensor distance measures for error calculations. The different mapping functions f_1 and f_2 investigated, linear and logarithmic, had little impact on the results. The overall observation is a decrease in the error for all values of α, compared to the error of the noisy tensor field.

The bilateral DT smoothing algorithm reduced the noise significantly and returned an output close (visually) to the original noise-free image. Fig. 2 presents quantitative analysis of noise reduction by measuring the average tensor distance between the noise-free data and the filtered image. To interpret these results it is insightful to provide an intuitive means of

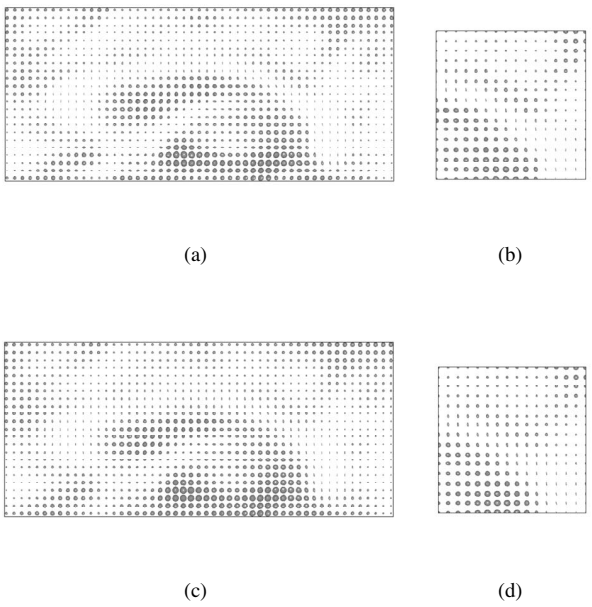

Fig. 5. Bilateral smoothing of the corpus callosum in brain DTMRI. Original and smoothed corpus callosum shown in a) and c) respectively. b) and d) show scaled up regions of the original and smoothed data respectively.

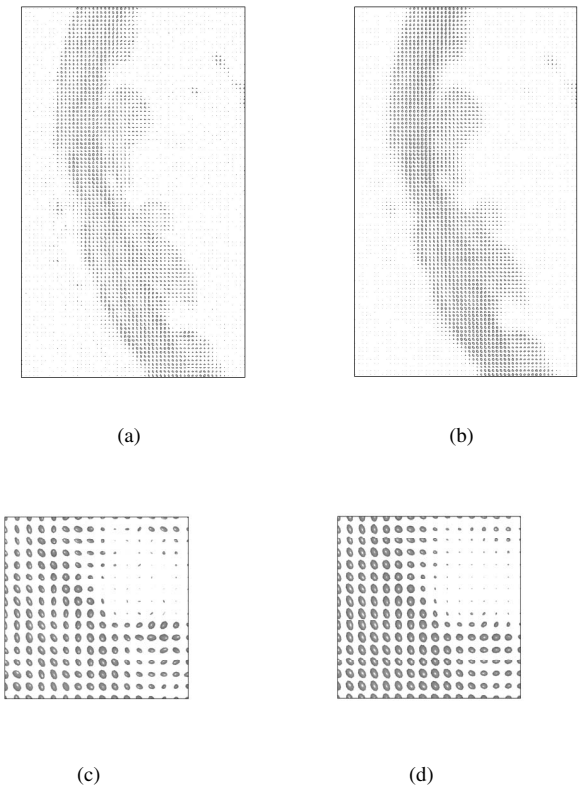

Fig. 6. Bilateral smoothing of the myocardium in cardiac DTMRI. Original and smoothed heart wall shown in a) and b) respectively. c) and d) show scaled up regions of the original and smoothed data respectively.

relating error values to DT differences (Fig. 4). Examples of cardiac and brain DTMRI smoothing results are presented in Fig. 5 and Fig. 6.

B. Effect of Number of Iterations on Bilateral DT-Smoothing

For a given α, the images were repeatedly smoothed (Fig. 3). Note the tendency of the error to decrease as the number of iterations is increased when smoothing the DT field without the interface. Also note the significant drop in error within the first 5 iterations. For the interface data, we also note a significant drop the first few iterations. However, a small gradual increase in error is observed as excessive iterations are performed. This is attributed to how smoothing will, to some small extent, blur the boundary (Fig. 3).

C. Interpolation

Interpolation of cardiac and brain DTMRI data is presented in Fig. 7. To quantitatively assess the interpolation, we compared the original data with the result of interpolation using a sub-sampled version of the original data. The error, calculated as the average tensor distance, d_{T_J}, over all voxels, was about 0.7 when every second DT was used to interpolate, compared to 1.41 with every sixth voxel. The corresponding values for $d_{T_{LE}}$ were 0.8 and 1.34.

IV. Conclusion

We aspire that the medical image analysis community will have access to accurate and practical diffusion tensor processing, analysis, and visualization tools at par with what is available for scalar fields. In this work we extend bilateral image filtering to diffusion tensor field data. We define diffusion tensor interpolation as a special case of bilateral tensor field filtering. Based on the proposed techniques, we provided encouraging quantitative and qualitative smoothing and interpolation results on simulated as well as real cardiac and brain DTMRI data. More extensive error analysis and validation, providing publicly available software implementation of these techniques, as well as extending other classical scalar image processing and analysis algorithms, are left for future work.

Acknowledgements

Drs. Patrick A. Helm and Raimond L. Winslow at the Center for Cardiovascular Bioinformatics and Modeling and Dr. Elliot McVeigh at the National Institute of Health for provision of the cardiac DTMRI data. Dr. Khader Hasan, Department of Diagnostic and Interventional Imaging, University of Texas Medical School at Houston, for provision of the brain DTMRI data.

References

[1] E. O. Stejskal and J. E.Tanner, "Spin diffusion measurements: spin echoes in the presence of a time-dependent field gradient," *J. Chem. Phys*, vol. 42, pp. 288–292, 1965.

[2] C.-F. Westin, S. E. Maier, H. Mamata, A. Nabavi, F. A. Jolesz, and R. Kikinis, "Processing and visualization of diffusion tensor mri," *Medical Image Analysis*, vol. 6(2), pp. 93–108, 2002.

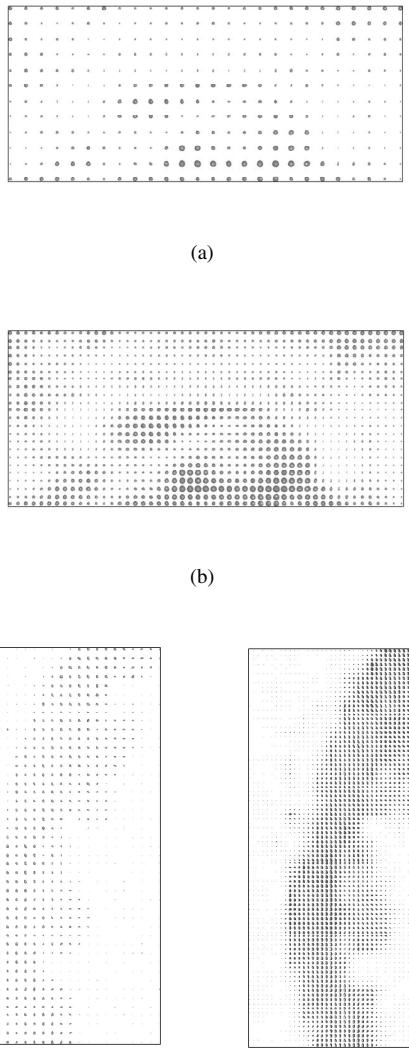

(a) (b) (c) (d)

Fig. 7. Interpolation examples of real brain and cardiac DTMRI data. a) and c) depict the coarse brain and heart data, while b) and d) show the corresponding interpolation results.

[3] M. Welk, C. Feddern, B. Burgeth, and J. Weickert, "Median filtering of tensor-valued images," in *Pattern Recognition*, ser. Lecture Notes in Computer Science, B. Michaelis and G. Krell, Eds., vol. 2781. Springer, Berlin, 2003, pp. 17–24.

[4] B. Burgeth, M. Welk, C. Feddern, and J. Weickert, "Morphological operations on matrix-valued images," in *Computer Vision - ECCV 2004*, ser. Lecture Notes in Computer Science, T. Pajdla and J. Matas, Eds. Springer, Berlin, 2004, vol. 3024, pp. 155–167.

[5] C. Castano-Moraga, M. A. Rodrigues-Florido, L. Alvarez, C.-F. Westin, and J. Ruiz-Alzola, "Anisotropic interpolation of dt-mri data," in *Seventh International Conference on Medical Image Computing and Computer-Assisted Intervention (MICCAI'04)*, Rennes - Saint Malo, France, 2004.

[6] J. Weickert and T. Brox, "Diffusion and regularization of vector- and matrix-valued images," in *Inverse Problems, Image Analysis, and Medical Imaging*, ser. Contemporary Mathematics, AMS, Providence, M. Z. Nashed and O. Scherzer, Eds., vol. 313, 2002, pp. 251–268.

[7] W. E. L. G. L. O'Donnell and C.-F. Westin, "Interface detection in dtmri," in *Seventh International Conference on Medical Image Computing and Computer-Assisted Intervention (MICCAI'04)*, Rennes - Saint Malo, France, 2004.

[8] Z. Wang and B. Vemuri, "An affine invariant tensor dissimilarity measure and its applications to tensor- valued image segmentation," *CVPR*, vol. (1), pp. 228–233, 2004.

[9] A. Brun, H. Knutsson, H. J. Park, M. E. Shenton, and C.-F. Westin, "Clustering fiber tracts using normalized cuts," in *Seventh International Conference on Medical Image Computing and Computer-Assisted Intervention (MICCAI'04)*, 2004, pp. 368–375.

[10] J. W. C. Feddern and B. Burgeth, "Level-set methods for tensor-valued images," in *Proc. Second IEEE Workshop on Variational, Geometric and Level Set Methods in Computer Vision*, O. Faugeras and N. Paragios, Eds., Nice, France.

[11] R. D. C. Lenglet and O. Faugeras, "Inferring white matter geometry from diffusion tensor mri: Application to connectivity mapping," in *ECCV*, vol. (4), 2004, pp. 127–140.

[12] M. R. C. Lenglet and R. Deriche, "Segmentation of 3d probability density fields by surface evolution: Application to diffusion mri," in *MICCAI*, vol. (1), 2004, pp. 18–25.

[13] C. Lenglet, M. Rousson, R. Deriche, O. Faugeras, S. Lehericy, and K. Ugurbil, "A riemannian approach to diffusion tensor images segmentation," in *IPMI*, 2005, pp. 591–602.

[14] C. L. M. Rousson and R. Deriche, "Level set and region based surface propagation for diffusion tensor mri segmentation," in *ECCV Workshops CVAMIA and MMBIA*, 2004, pp. 123–134.

[15] D. T. R. Deriche and C. Lenglet, "Dt-mri estimation, regularization and fiber tractography," in *ISBI 2004*, 2004, pp. 9–12.

[16] M. Wiegell, D. Tuch, H. Larson, and V. Wedeen, "Automatic segmentation of thalamic nuclei from diffusion tensor magnetic resonance imaging," *NeuroImage*, vol. 19, pp. 391–402, 2003.

[17] P. B. D. Alexander, C. Pierpaoli and J. Gee, "Spatial transformations of diffusion tensor magnetic resonance images," *IEEE Trans. Med. Imag.*, vol. 20, pp. 1131–1139, Nov. 2001.

[18] J. Ruiz-Alzola, C.-F. Westin, S. K. Warfield, C. Alberola, S. E. Maier, and R. Kikinis, "Nonrigid registration of 3d tensor medical data," *Medical Image Analysis*, vol. 6, pp. 143–161, 2002.

[19] A. Guimond, C. R. G. Guttmann, S. K. Warfield, and C.-F. Westin, "Deformable registration of dt-mri data based on transformation invariant tensor characteristics," in *ISBI*, Washington (DC), USA, 2002.

[20] I. F. Talos, L. O'Donnell, C.-F. Westin, S. K. Warfield, W. M. Wells, S. S. Yoo, L. Panych, A. Golby, H. Mamata, S. E. Maier, P. Ratiu, C. G. Guttmann, P. M. L. Black, F. A. Jolesz, and R. Kikinis, "Diffusion tensor and functional mri fusion with anatomical mri for image guided neurosurgery," in *Sixth International Conference on Medical Image Computing and Computer-Assisted Intervention (MICCAI'03)*, Montreal, Canada, 2003.

[21] C. Tomasi and R. Manduchi, "Bilateral filtering for gray and color images," in *Sixth International Conference on Computer Vision*, 4-7 Jan 1998, pp. 839–846, digital Object Identifier 10.1109/ICCV.1998.710815.

[22] C. A. C.K. Wilbur and C. Simon, "Trilateral filtering for biomedical images," in *Proceedings of the IEEE International Symposium on Biomedical Imaging: From Nano to Macro*, 2004, pp. 820–823.

[23] P. F. Xavier Pennec and N. Ayache, "A riemannian framework for tensor computing," *International Journal of Computer Vision*, vol. 65(1), Oct. 2005, note: To appear. Also as INRIA Research Report 5255.

[24] S. J. P.T. Fletcher, "Principal geodesic analysis on symmetric spaces: Statistics of diffusion tensors," ser. Lecture Notes in Computer Science, vol. 3117. Springer-Verlag, 2004, pp. 87–98.

[25] X. P. V. Arsigny, P. Fillard and N. Ayache, "Fast and simple calculus on tensors in the log-euclidean framework," in *Proceedings of MICCAI'05*, ser. Lecture Notes in Computer Science, J. Duncan and G. Gerig, Eds. Palm Springs, California: Springer Verlag, Oct. 2005, to Appear.

[26] R. B. E. Yoruk, B. Acar, "A physical modal for dt-mri based connectivity map computation," in *Proceedings of MICCAI'05*, ser. Lecture Notes in Computer Science, J. Duncan and G. Gerig, Eds. Springer Verlag, 2005, pp. 213–220.

[27] S. F.Witelson, "Hand and sex differences in the isthmus and genu of the human corpus callosum: A postmortem morphological study," *Brain*, vol. 112, pp. 799–835, 1989.

[28] H. KM, R. Gupta, R. Santos, J. Wolinsky, and P. Narayana, "Fractional diffusion tensor anisotropy of the seven segments of the normal-appearing white matter of the corpus callosum in healthy adults and relapsing remitting multiple sclerosis," *Journal of Magnetic Resonance Imaging*, vol. 21(6), pp. 735–743, 2005.